Renewable Energy 128 (2018) 432–443

Contents lists available at ScienceDirect

Renewable Energy

journal homepage: www.elsevier.com/locate/renene

Development of a solar irradiance dataset for Oahu, Hawai'i

Sarah Williamson [a, *], Steven Businger [a], Dax Matthews [b]

[a] Department of Atmospheric Sciences, University of Hawai'i at Manoa, Honolulu, Hawai'i, USA
[b] Hawai'i Natural Energy Institute, University of Hawai'i at Manoa, Honolulu, Hawai'i, USA

ARTICLE INFO

Article history:
Received 13 February 2018
Accepted 23 May 2018
Available online 24 May 2018

Keywords:
Solar irradiance modeling
Solar energy
Hawaii
HELIOSAT
Temporal and spatial variability
Satellite imagery

ABSTRACT

Solar power as an alternative energy source in Hawai'i has grown in recent years [1], with increasing amounts of photovoltaic panels found statewide. Power resource management and grid stability require that the variability in irradiance, hence, solar power coming into the electric grid be understood. The aim of this study is to produce an irradiance dataset for Oahu, Hawai'i, containing temporal and spatial variability, so it can be used in modeling power generation.

Images from the Geostationary Operational Environmental Satellite are used to estimate surface irradiance within the Heliosat method and are validated against ground-based pyranometer measurements. The diurnal cycle was then removed to assess the accuracy of the Heliosat method in estimating atmospheric attenuation. Lastly, the irradiance data was converted into DC power to consider the dataset in terms of power generation.

The irradiance dataset produced has RMSE values of 15–30% depending on location, with correction for viewing angle discrepancies found to improve the performance. Variability on sub hourly, diurnal, monthly and yearly time scales are found within the dataset, as well as events such as an El Nino year, a La Nina year and Kona lows, together with a spatial distribution consistent with previous research.

1. Introduction

It is important to understand the spatial and temporal variability of irradiance, as this has applications in a variety of fields such as alternative energy, climate change and agriculture. In particular, the use of solar power as an alternative energy source in Hawai'i has grown in recent years [1], with increased amounts of photovoltaic (PV) panels found island wide and this is only set to continue. Therefore variability in irradiance, which leads to variability in power coming into the electric grid, needs to be understood for the purpose of power resource management and grid stability.

Temporal (daily, monthly and annual) and spatial variability in irradiance has been analyzed on both a regional and global scale. Regional studies use either ground-based measurements (e.g. [2,3]) or irradiance estimates derived from satellites (e.g. [4–6]) to analyze the temporal and spatial features of global, direct and diffuse irradiance over various timescales to gain a better understanding of its behavior in a particular region. There are also studies that have been conducted using sites spread across the globe (e.g. [7–9]) using ground-based measurements to assess global trends, though these are not as common.

Numerous studies have considered variability in irradiance on sub hourly timescales (e.g. [10–12]). The magnitude and frequency of fluctuations in irradiance on these timescales are analyzed to find the underlying trends within the dataset, typically for multiple locations. Generally, variation in irradiance is caused by changes in the amount of radiation reaching the ground due to the transparency of the atmosphere, which can be affected by clouds, aerosols, location and time of year.

The topography of Oahu has a strong effect on cloud formation and hence surface irradiance. The Ko'olau mountain range runs close to the east coast of the island, whilst the Wai'anae mountain range is found on the west side. The east coast of the island is often referred to as the windward side due to the prevailing north easterly trade winds, whilst the west coast is referred to as the leeward side. For the majority of the year, trade winds cause cloud formation above the Ko'olau mountain range due to orographic lifting [13]. As a result, the flat coastal plains found south of the Wai'anae mountain range on the leeward side tend to experience less cloudy conditions compared to the rest of the island. In the winter however, Kona (leeward) winds often disrupt the trade winds causing cloud formation on the leeward side of the island [11,14,15].

* Corresponding author.
E-mail addresses: sarahw4@hawaii.edu (S. Williamson), businger@hawaii.edu (S. Businger), daxm@hawaii.edu (D. Matthews).

https://doi.org/10.1016/j.renene.2018.05.082
0960-1481/

There have been a number of studies focused on irradiance in Hawai'i. Bryce et al., 2018 [6] used the National Solar Radiation Database (NSRDB) produced by the National Renewable Energy Laboratory (NREL) in order to recommend using a multi-year irradiance dataset as opposed to a single year dataset when modeling power generation, as there was found to be significant monthly, annual and seasonal variability which would not be captured in a single year dataset.

Giambelluca et al., 2014 [14] estimated the mean annual cycle and the mean diurnal cycle of solar irradiance across Hawai'i as part of a larger project. They combined estimates from the REST2 clear sky radiation model with output from a statistical function derived from ground-based measurements as well as satellite derived cloud cover, to produce solar irradiance.

Irradiance at high elevation sites in Hawai'i has been considered by Longman et al. [16–18] on the islands of Maui and Hawai'i. Different approaches were tested to parameterize a clear sky radiation model [17] and a method has been presented for homogenizing long term measurements of irradiance, using modeled clear sky estimates to identify discontinuities [18]. The temporal change in irradiance at these sites was also discussed, with trends being identified between the Hawaiian wet and dry seasons [16].

Geostationary satellites are a valuable resource when investigating irradiance. They allow estimates of irradiance in locations where ground-based sensing equipment does not exist, as well as being able to determine irradiance estimates on a fine temporal and spatial scale. It has even been suggested that solar irradiance maps obtained using satellite images can be more accurate than the interpolation of measurements made at ground level [19,47].

There are many techniques that have been developed to estimate surface irradiance using geostationary satellite data, this being one of the most extended approaches [20,21]. These can take the form of statistical or physical models [21–23]. Statistical models rely on statistical regression between satellite data and ground measurement data, and do not require detailed information on the composition of the atmosphere. Physical models however require this information in order to model the attenuation of irradiance through the atmosphere.

Due to the high resolution of the Geostationary Operational Environmental Satellite (GOES) and Meteorological Satellite (METEOSAT) products, there have been many methods developed using this data. The earliest methods were developed by Gautier et al., 1980 [24] who used a physical model with GOES imagery and Cano et al., 1986 [25] who used a statistical model with METEOSAT imagery. Methods have since progressed to incorporate atmospheric parameter information, radiative transfer and the removal on reliance on empirical parameters [26–28].

The method developed by Cano et al., 1986 [25] is called the Heliosat method and is one of the most established schemes which has been widely and successfully tested against ground data, producing accurate results [29–31]. The method uses the digital counts recorded by the satellite and converts them into a cloud cover index, which is then used in a statistical estimation of global radiation [25]. There have since been many modifications to the original method. Heliosat 1 introduced a linear empirically defined relationship between the cloud index and the clearness index, with ground-based measurements being used to tune the method during development [31]. Heliosat 2 reduces the number of empirically defined parameters, expressing them using known physical laws and parameters. It also uses calibrated counts of the satellite image which are then converted into radiances to take into account the change of sensor, removing the need for ground measurements to tune the model [32].

Currently the only known historic irradiance dataset for Hawai'i is provided by the NSRDB at a spatial resolution of 4 km and a temporal resolution of 30-min. Using data from GOES-West, this study aims to produce a finer resolution historic dataset for Oahu, Hawai'i at a spatial resolution of 1 km and a temporal resolution of 15-min, to be able to explore variability in irradiance on Oahu on finer scales and for use in modeling power generation. To do this, the Heliosat method originally proposed by Cano et al. [25] and later modified by Beyer et al. [31] and Hammer et al. [29] was used for data between the years 2006 and 2016.

The remainder of this document is organized as follows: Section 2 discusses the version of the Heliosat method used and the conversion from irradiance into power is briefly discussed. Section 3 describes the satellite data, meteorological data and ground-based pyranometer data used in the study. Section 4 compares the Heliosat method output to ground-based pyranometer data to assess the accuracy of the method. Section 5 discusses what further information can be extracted about irradiance on Oahu using this dataset, examining temporal variability on varying scales and how it in turn would affect power coming onto the electric grid. Section 6 presents a summary of the work with conclusions and considerations for future work.

2. Methods

2.1. Heliosat method

For this study, the Heliosat method originally proposed by Cano et al. [25] and later modified by Beyer et al. [31] and Hammer et al. [29] is used, with imagery from GOES-West.

2.2. Clear sky irradiance

This version of the method calculates the direct and diffuse clear sky irradiance separately using two empirically defined models ([33,34], resp.), incorporating the Linke turbidity factor to take into account atmospheric turbidity. The direct normal clear sky irradiance $G_{dn,clear}$ is given by:

$$G_{dn,clear} = G_{sc}\epsilon e^{-0.8662T_L\delta_R(m)m} \tag{1}$$

where G_{sc} is the direct normal solar radiation, ϵ is the eccentricity correction, T_L is the Linke turbidity factor and $\delta_R(m)$ is the Rayleigh optical thickness and m is the air mass.

The diffuse clear sky irradiance $G_{diff,\ clear}$ is given by:

$$G_{diff,clear} = G_{ext}\varepsilon\Big(0.0065 + (-0.045 + 0.0646T_L)\cos(\theta_Z) + (0.014 - 0.0327T_L)\cos^2(\theta_Z)\Big) \tag{2}$$

where G_{ext} is the extraterrestrial irradiance on a horizontal plane and θ_Z is the zenith angle of the sun (degrees). The direct and diffuse clear sky irradiance is then added to find the total clear sky irradiance:

$$G_{clear} = G_{dn,clear}\cos(\theta_Z) + G_{diff,clear} \tag{3}$$

2.3. Cloud cover

Relative reflectance or albedo, ρ, is calculated using:

$$\rho = \frac{C - C_0}{G_{ext}} \tag{4}$$

where C is the pixel intensity measured by the satellite radiometer,

G_{ext} is the extraterrestrial solar radiation on the horizontal plane, and C_0 is the sum of the instrument offset and the atmospheric offset due to atmospheric backscattering.

The cloud cover index, n, is introduced defined using the relative reflectance from Eq. (4):

$$n = \frac{\rho - \rho_{min}}{\rho_{max} - \rho_{min}} \tag{5}$$

where ρ_{min} is the surface reflectance and ρ_{max} is the maximum reflectance. The surface reflectance is found by a monthly analysis of the dark pixels, so as to account for seasonal variability. The maximum reflectance is calculated separately for each satellite radiometer. The cloud cover index varies between 0 and 1, where 0 indicates cloudy conditions and 1 indicates clear skies. The cloud cover index is then used to calculate the clear sky index (K^*_T) using the relationship derived in [35];

$$\begin{array}{ll} n \le -0.2 & K^*_T = 1.2 \\ -0.2 < n \le 0.8 & K^*_T = 1 - n \\ 0.8 < n \le 1.1 & K^*_T = 2.0667 - 3.6667\ n + 1.66672\ n^2 \\ 1.1 < n & K^*_T = 0.05 \end{array} \tag{6}$$

The surface irradiance, G, can now be defined as the product of the clear sky irradiance and the clear sky index:

$$G = K^*\ G_{clear} \tag{7}$$

An additional correction is made for viewing angle discrepancies, arising where the satellite perceives the cloud shadow to be in a different location than in reality due to the angle of the sun/satellite. To account for this, the cloud top height (CTH) for each pixel is used to interpolate the surface irradiance to its new location, which is calculated using the cloud height and solar geometry.

2.4. PV Watts Version 5

The conversion from irradiance into DC power is achieved using the PV Watts Version 5 module from the System Advisory Model (SAM) developed by NREL, which estimates the electricity production of a grid connected photovoltaic system based on a number of inputs [36]. It requires temperature and wind speed data (described in Section 3.3) as well as the direct normal irradiance and diffuse horizontal irradiance for a location. Parameters for the photovoltaic (PV) system configuration can be specified, however for this study default values are used by the module, shown in Table 1.

3. Data

3.1. Satellite imagery

Satellite imagery from GOES-West were collected for the period 2006 to 2016 for Oahu, Hawai'i' at 1 km spatial resolution and 15-min temporal resolution. However, data was unavailable for certain times, most noticeably during 2010, 2012, July 2014 and April/May in 2015. An example visible GOES-West satellite image is shown in Fig. 1.

Table 1
PV system configuration.

System Capacity (kW DC)	4
DC/AC ratio	1.1
Tilt of system (deg)	20
Azimuth angle (deg)	180
Inverter efficiency	96
System losses (%)	14.0757
Fixed tilt system	Yes
Ground coverage ratio	0.4

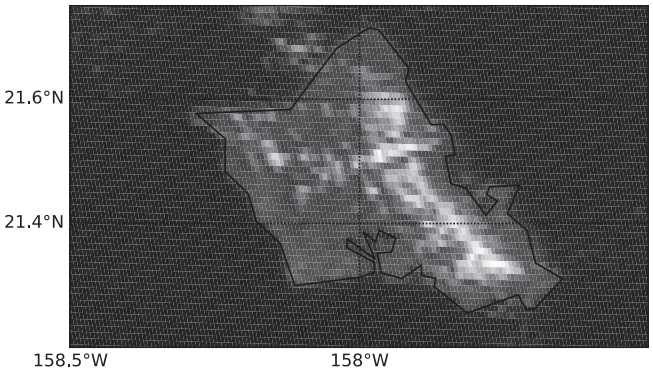

Fig. 1. Example GOES visible radiance image at 10:15 a.m. on 29th July 2006.

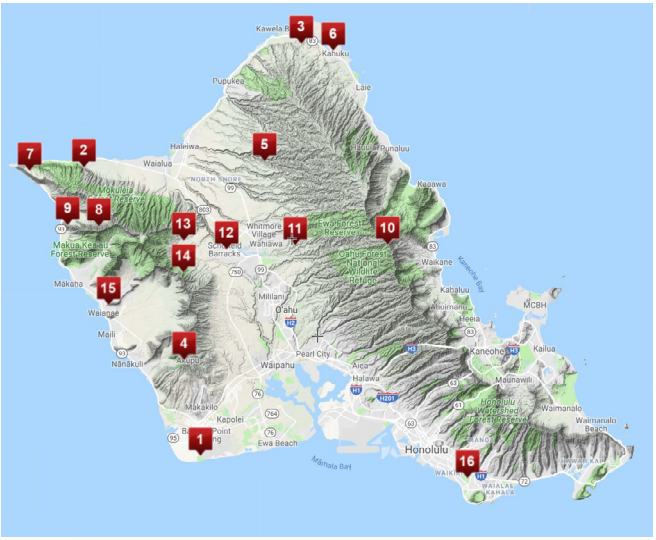

Fig. 2. Map of Oahu showing validation station locations as listed in Table 3.

Cloud top height (CTH) data was available between 2012 and 2016. CTH maps used were from the Space Science and Engineering Center at the University of Wisconsin as well as being estimated from GOES-West imagery using the infrared window (IRW) technique, for further details see [37].

3.2. Validation station data

We validate the satellite data using irradiance data provided from three different sources of ground-based stations. All data has undergone basic quality checks, including the removal of outliers, the defaulting of night time values to 0 and a visual check to ensure the irradiance data displays the expected behavior. The locations of all sites can be seen in Fig. 2, with further information shown in Tables 2 and 3.

3.2.1. Remote automatic weather stations (RAWS)

The RAWS network is operated by the National Interagency Fire Center. Irradiance data for the 14 stations located on Oahu, Hawai'i was obtained from [38] in the form of hourly averages which had been calculated for each station using the 60 measurements taken

Table 2
Description of pyranometers.

Site	Brand	PV module	Number of sensors	Sensor accuracy (%)
RAWS network	LI-COR	LI-200A	1	±5
Kalaeloa NREL sites	LI-COR	LI-200	17	±5
UH Manoa	Mesotech	SP-LITE	1	±5
UH Manoa	YES	TSP-400	2	±3
UH Manoa	Apogee	SP-110	20	±5

in the preceding hour (one per minute). Further details are found in [38–40].

3.2.2. NREL network

The NREL Measurement and Instrumentation Data Center (MIDC) provides irradiance data for numerous stations in the US. Irradiance data for 17 stations located within a 1 km radius at Kalaeloa Airport, Oahu was obtained from [41], at 1-min resolution. Due to their close proximity, the data from all 17 stations was averaged to get a 15-min time series, using all measurements taken in the previous 15-min. Further details are found in [40,42,43].

3.2.3. University of Hawai'i at manoa (UH manoa)

Irradiance data from a group of pyranometers operated by the Hawai'i Natural Energy Institute (HNEI) located at the Hawai'i Institute of Geophysics at UH Manoa was obtained. The data is at 1-s resolution, so to keep these data consistent with the satellite data, a 15-min average was calculated using all measurements taken in the previous 15-min. Further details are found in [11,44].

3.3. Meteorological data used within PV Watts

Meteorological data was obtained from [45] for a weather station located at Kalaeloa Airport, operated by the National Weather Service (NWS) and Federal Aviation Administration (FAA). The format of the data provided are hourly temperature and wind speed values at 2 m and 10 m respectively. Higher temporal resolution temperature and wind speed data is also available for 2010–2011 from NREL [43] at this site at 1-min intervals. To coincide with the satellite data, the temperature and wind speed values every 15-min were used.

4. Validation

- In this section we compare the satellite irradiance data to the ground-based pyranometer (station) data. As a measure of comparison, we use the root mean square error (RMSE) and the correlation coefficient (CC) defined as:

$$RMSE(x,y) = \sqrt{\frac{1}{N}\sum_{i=1}^{N}(x_i - y_i)^2} \tag{8}$$

and

$$CC(x,y) = \frac{\sum_{i=1}^{N} x_i y_i}{\sqrt{\sum_{i=1}^{N} x_i^2 \sum_{i=1}^{N} y_i^2}} \tag{9}$$

where N is the number of station data points and x are the satellite irradiance data at the same location and time as the station data y. The RMSE is then normalized by the peak satellite data value over the time period being analyzed. The RMSE provides a measure of the difference between the satellite irradiance data and the station data while the CC determines the strength of the relationship between the two datasets.

4.1. Estimation of satellite data at station locations

Ideally, the station data used to validate the satellite irradiance data would have the same temporal and spatial resolution. However, as the satellite is on a 1 km grid, the Barnes Analysis method [46] is used to interpolate the data to the station locations. The method is a distance weighted mean of nearby grid points and produced consistently higher CC and lower RMSE values when compared with a simple nearest-neighbor approach.

4.2. Validation

The RMSE and CC calculated for all coincident satellite and station data at each station location is shown in Table 4. Performance varies between stations, with Station 1 performing the best with a RMSE of 15.1% and a CC of 0.95, whilst Station 10 has the poorest performance with a RMSE of 30.4% and a CC of 0.78.

Figs. 3 and 4 shows the mean monthly CC and RMSE between

Table 3
Details of stations used for satellite data validation.

Station number	Station name	Elevation (m)	Time period	Resolution
1	Kalaeloa	11	03/2010–10/2011	15 min[a]
2	Dillingham	31	01/2006–12/2014	60 min
3	Kahuku Training Area	182	01/2006–12/2014	60 min
4	Palehua	722	03/2009–12/2014	60 min
5	Kawailoa Training area	388	01/2006–01/2007	60 min
6	Kii	2	01/2006–12/2014	60 min
7	Kuaokala	267	06/2010–12/2014	60 min
8	Makua Valley	158	01/2006–12/2014	60 min
9	Makua Range	6	01/2006–12/2014	60 min
10	Oahu Forest NWR	699	08/2006–12/2014	60 min
11	Schofield East	381	01/2006–12/2014	60 min
12	Schofield Barracks	299	01/2006–12/2014	60 min
13	Schofield Firebreak	347	01/2006–12/2014[b]	60 min
14	Schofield South Range	454	01/2006–05/2014[b]	60 min
15	Waianae Valley	292	01/2006–12/2014	60 min
16	UH Manoa	54	01/2015–07/2016	15 min[a]

[a] Indicates resolution used.
[b] Indicates intermittent data.

Table 4
RMSE and CC for all coincident irradiance data for each station.

Station number	RMSE (%)	CC	Number of records
1	15.1	0.95	15736
2	19.8	0.91	15068
3	16.2	0.94	30459
4	19.6	0.91	16130
5	19.3	0.93	3952
6	15.9	0.94	28992
7	18.0	0.92	12326
8	20.2	0.91	8628
9	23.7	0.87	25572
10	30.4	0.78	27418
11	19.0	0.92	18068
12	21.5	0.89	27186
13	21.1	0.91	18275
14	25.5	0.87	17341
15	24.0	0.87	29833
16	18.2	0.92	8170

the satellite and station data as a time series. To calculate this, the CC and RMSE are computed for each month for individual stations, then averaged to produce a single value. In 2015/2016, data was available from only one station, hence the CC and RMSE values during this time are single values.

The mean CC ranges from 0.8 to 0.97 throughout the time period, with an overall mean of 0.91, whilst the mean RMSE ranges from 11% to 35%, with a mean of 24% over the entire time period. The data shows consistent combined performance for all stations over time, supporting the results in Table 4.

Separating the data into those time periods which have CTH available and those which do not, the periods with it incorporated i.e. that take into account discrepancies in viewing angle, perform better with an overall mean RMSE of 23.9% compared to 24.4%.

The difference between the mean satellite and mean station irradiance data for all stations as a function of hour of day and month of year is shown in Fig. 5. Positive values indicate that the satellite data is greater than the station data. The satellite data is typically greater than the station data earlier in the day, and by late afternoon the reverse is observed and the station data is higher. In the first half of the year the difference between the two datasets is smaller in the mornings than the afternoons, whilst during the second half of the year the difference is highest around midday but close to zero in the later afternoon/evening.

The net effect of this is apparent when considering the total difference between the two datasets per month or per hour. When viewed per month the satellite data is lower than the station data from January to March and is greater than the station data for the rest of the year, with the peak difference in October. Viewed per hour, the satellite data is lower than the station data from 15:00 onwards and is greater than the station data earlier in the day, with the peak difference in the 11:00 h. This suggests that there is a seasonal variability that is not taken into consideration within the satellite data.

The mean spatial satellite irradiance calculated at 10:00 HST for all available data is shown in Fig. 6. This is consistent with what is known about the spatial distribution of irradiance on Oahu, as described in Section 1. The clouds which form above the Ko'olau mountain range can be seen from the low levels of irradiance in the area. Further south on the leeward side the flat coastal plains are identifiable through higher levels of irradiance, reflecting the less cloudy conditions experienced on this side of the island. This behavior is also seen in the visible GOES-West satellite image (Fig. 1) by high radiance values (dark regions) over the coastal plains, indicating clear sky while low values (bright regions) over the mountain ranges indicate cloud cover.

Fig. 6 also shows lower levels of irradiance north of the coastal plains on the leeward side located along the Waianae mountain range that is not seen in the example given in Fig. 1. This is caused by those periods when Kona winds disrupt the trade winds, causing clouds to form above the Wai'anae mountain range [11,14,15].

4.3. Validation discussion

We find that the satellite irradiance data performs well in comparison with previous studies, with RMSE values of 15–30%, compared with values of 20–25% [47] and 17–25% [48] for varying types of satellite based estimation schemes and 14–30% [32] for those using the Heliosat 1 method (when compared with ground-

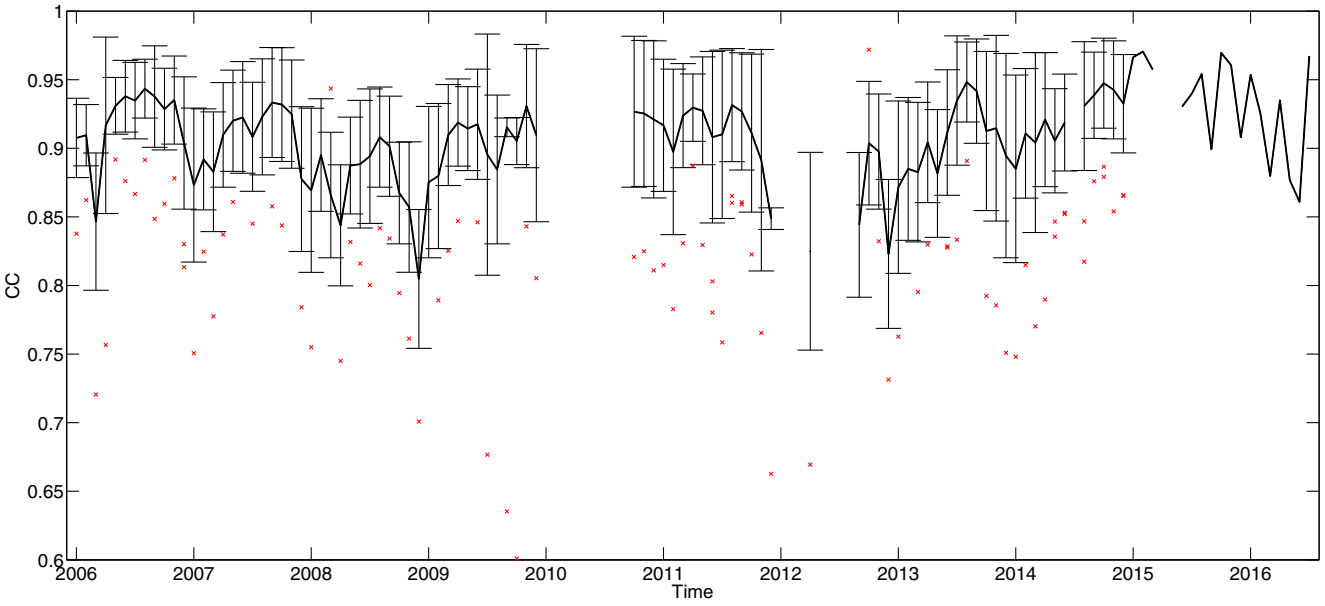

Fig. 3. Mean monthly CC values between all coincident satellite and station data shown as a time series for all stations. Error bars are ± 1 standard deviation (σ). Outliers are defined as those values further than 1.5σ from the mean. Gaps indicate missing data.

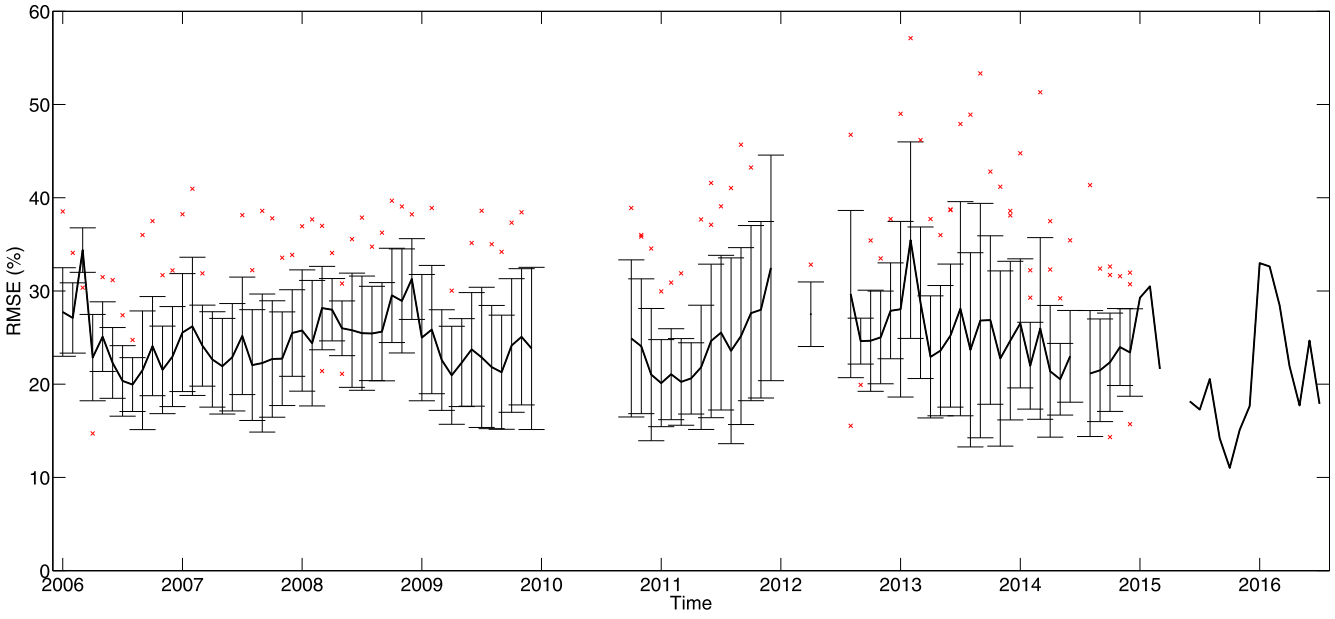

Fig. 4. Mean monthly RMSE values between all coincident satellite and station data shown as a time series for all stations. Error bars are ± 1 standard deviation (σ). Outliers are defined as those values further than 1.5σ from the mean. Gaps indicate missing data.

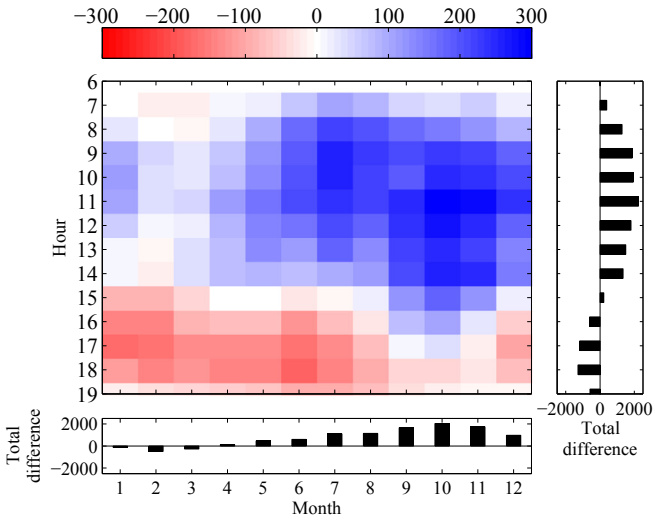

Fig. 5. The difference between the mean satellite and mean station irradiance data in W/m^2 for all stations for all available data per hour of day and month of year. The total difference per month and per hour is shown in the bar charts on the x and y axis respectively.

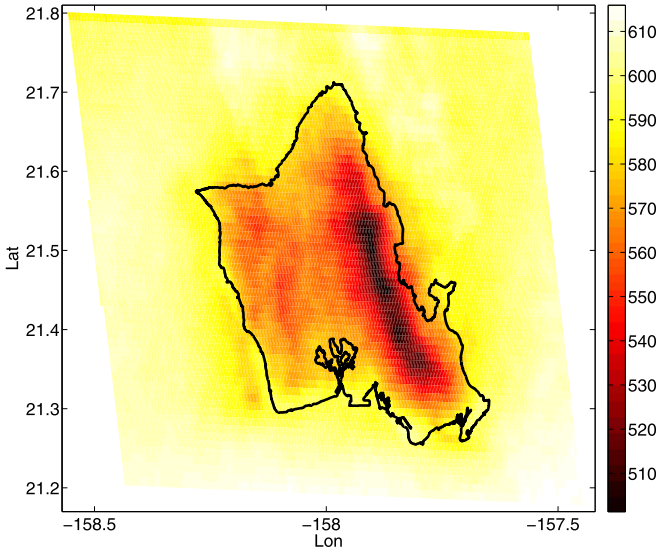

Fig. 6. Mean spatial satellite irradiance (W/m^2) over Oahu at 10:00 HST, calculated using all available data.

based measurements). Additionally, CC values are consistently good ranging from 0.78 to 0.95. Correcting for viewing angle discrepancies is found to improve the performance of the satellite data, showing the importance of taking into account and correcting for the effect of cloud shadows on surface irradiance.

Reasons for the discrepancies between the satellite and station data can be separated into three groups [47]. First are those from assumptions made during the conversion of the satellite imagery into irradiance, as well as satellite measurement errors. The individual station RMSE values reported in Table 4 do not show a consistent temporal or spatial pattern to suggest that the difference in performance between stations could be easily corrected in satellite data. Rather it is a result of the variability in irradiance found in each location.

Second includes errors in the pyranometer measurements used for validation. Basic quality checks (described in Section 3.2) have been carried out on the station data to try to minimize any errors. Accuracies for individual sensors are 3–5% (Table 2) which agrees with those found in literature [47].

Third are those errors which come from comparing different spatial and temporal measurements. Spatially, the 1 km grid satellite data means that any cloud smaller than the image pixel is averaged with the clear sky also in that grid cell, causing the resulting irradiance to lie between clear and cloudy. This means that the satellite data would not capture small-scale variability that is seen in the single point ground measurements of the station data. Temporally, the station data are average values that have been calculated using data over the preceding 15-min or hour, whilst the

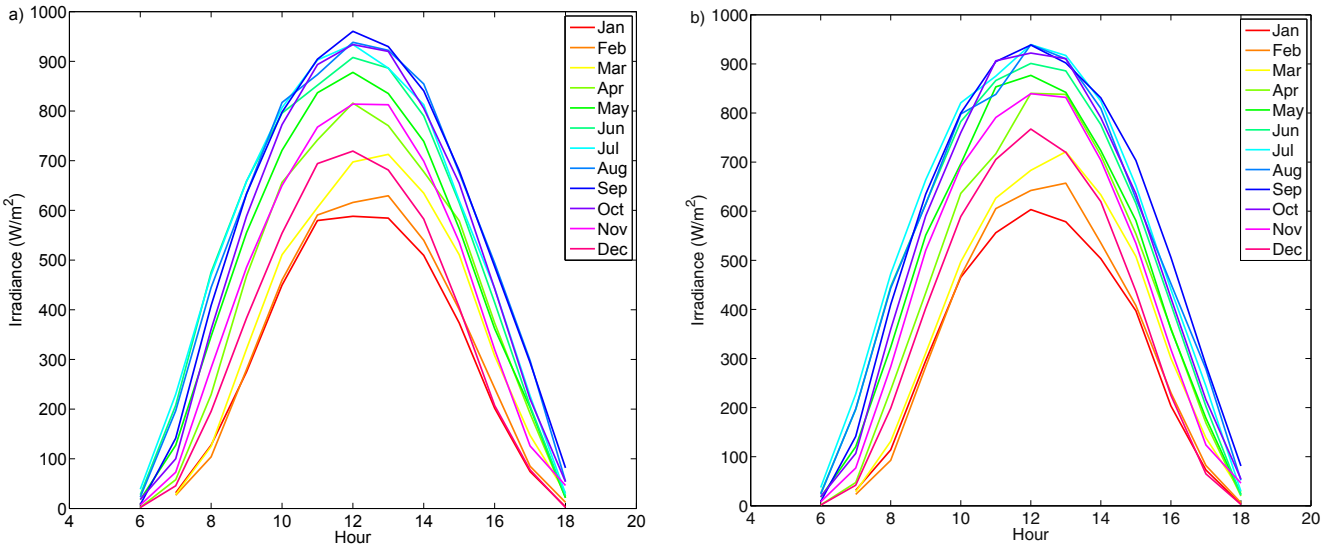

Fig. 7. Mean diurnal irradiance as a function of month for Station 1 for (a) 2007 and (b) 2011.

satellite data is also an average made from the time it takes the satellite to scan the island. This means that these values may be more representative of conditions at another point during the time period being averaged over, rather than at the end of the time period, where the data is assigned. Thus when coincident values between the satellite and station data are compared, differences may be seen as each dataset may not be accurately describing the irradiance at that time.

5. Analysis and discussion

To understand what else can be learned about irradiance from the satellite dataset, we now focus on Station 1 at Kalaeloa. This station was chosen as it is located on the leeward side of Oahu, in an area of flat topography with less cloudy conditions, resulting in higher levels of irradiance compared to elsewhere on the island. These conditions have also led to the development of solar farms in this area, such as Kalaeloa Renewable Energy Park, Kalaeloa Solar II and Kapolei Sustainable Energy Park.

5.1. Monthly and yearly variability

To look at the variation between years, the diurnal cycle for each month can be considered, for example Fig. 7. Each year exhibits similar behavior, with lower irradiance in winter months (December to April) and higher irradiance in the summer months (May to November) as would be expected, with peak irradiance values being similar between years.

The yearly variation in each month can also be considered, for example Fig. 8. Irradiance in the winter months show higher levels of variability compared to the summer months, due to the amount of cloud cover varying in the winter months between each year. There is less cloud clover found during the summer months, hence these times show less variability between years.

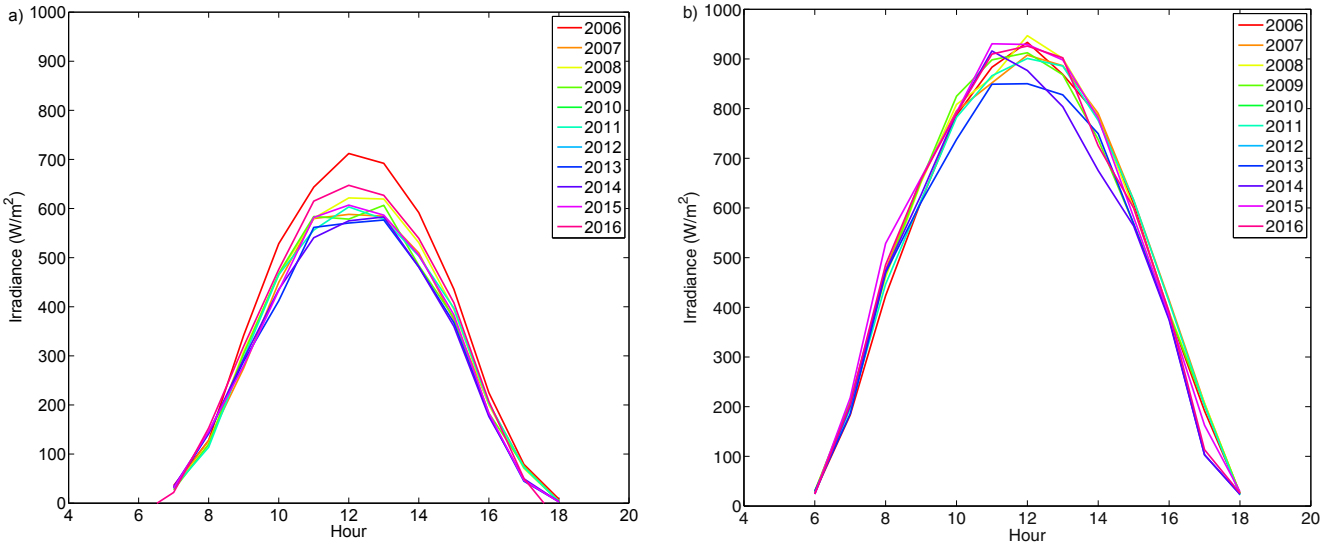

Fig. 8. Mean diurnal irradiance as a function of year for Station 1 for (a) January and (b) June.

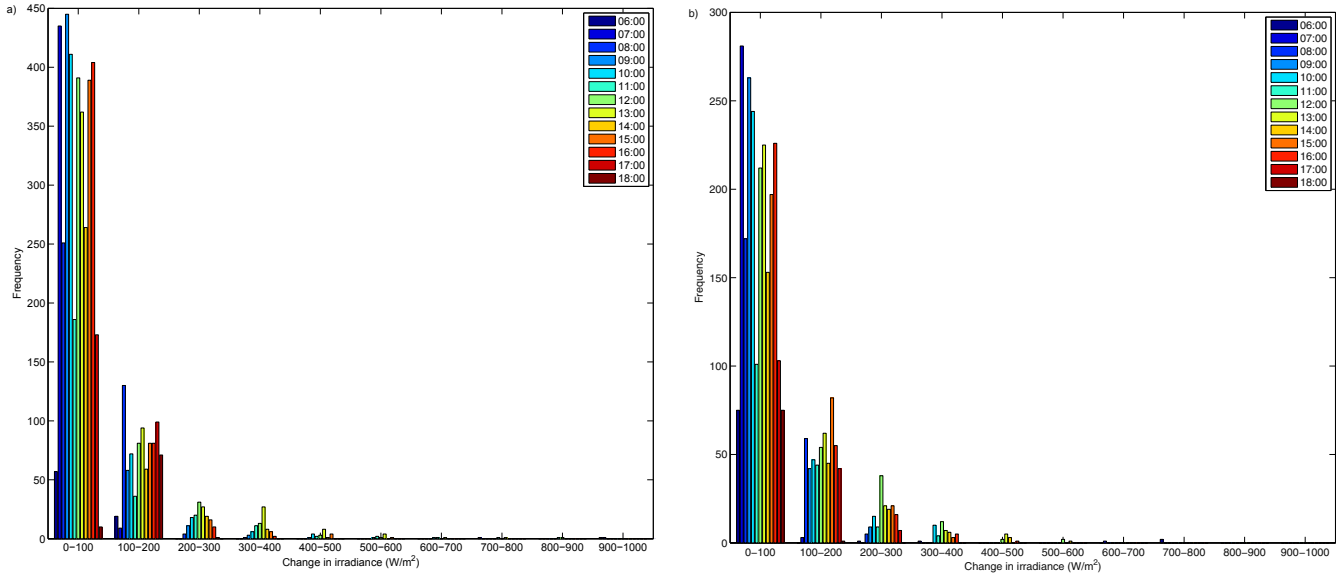

Fig. 9. Frequency of changes in (a) satellite irradiance and (b) station irradiance data ordered by magnitude and separated by hour, for Station 1 in 2010 and 2011.

5.2. Short term variability

Short term variability in irradiance, which leads to variability in power coming into the electric grid, is important to understand for grid stability. We now look at how well the satellite data is able to capture short term variability, by considering the change in irradiance occurring every 15-min for both satellite and station data during 2010 and 2011. The change was calculated by:

$$\Delta x = |x_{t+1} - x_t| \tag{10}$$

where x_t is the irradiance at time t and x_{t+1} is the irradiance at time $(t+1)$. The resulting output is then ordered according to the magnitude of the change.

Breaking the changes down by hour, shown in Fig. 9, lower magnitude changes (0 W/m^2 to 200 W/m^2) exist in both datasets in the early mornings and late afternoons, as consistent with the

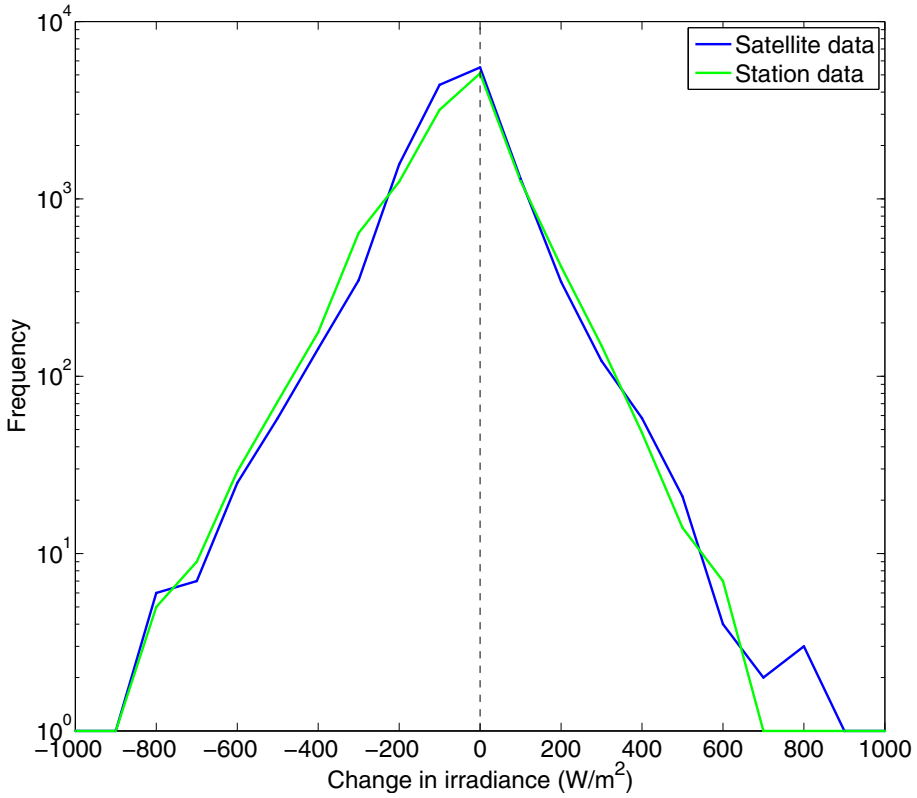

Fig. 10. Frequency of changes in irradiance ordered by magnitude, showing sign of change for Station 1 in 2010 and 2011.

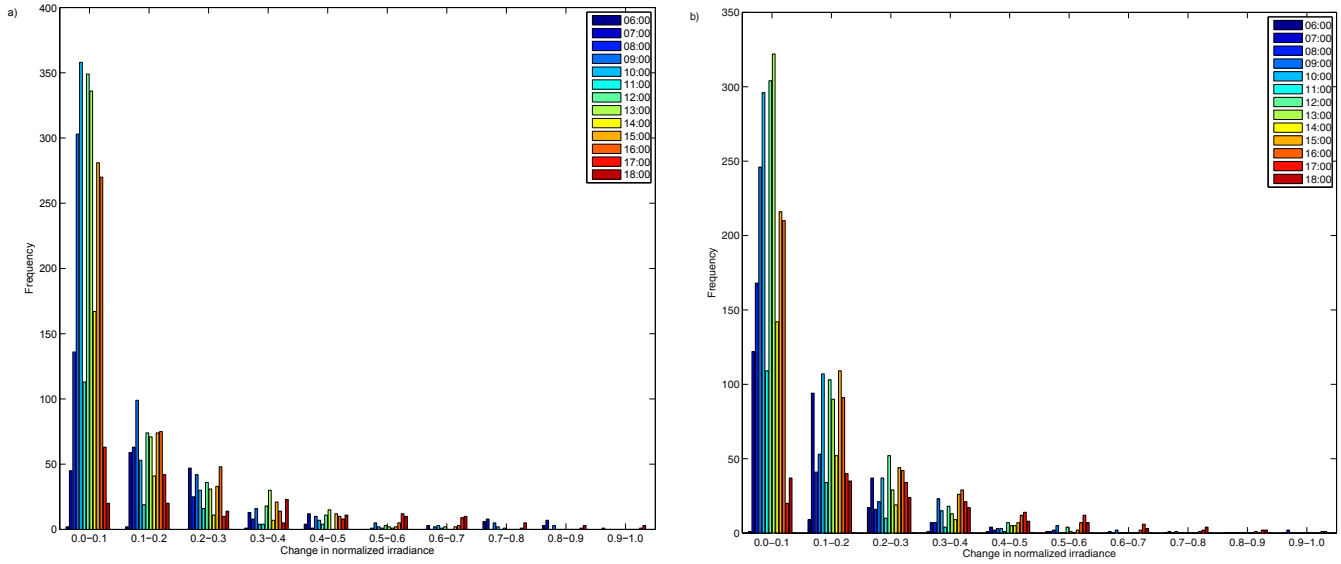

Fig. 11. Frequency of changes in (a) normalized satellite irradiance data and (b) normalized station irradiance data ordered by magnitude and separated by hour, for Station 1 in 2010 and 2011.

diurnal cycle. Conversely, levels of variability in irradiance greater than 200 W/m^2 are more frequently seen around midday/early afternoon. This behavior is likely due to passing clouds and is consistent with behavior seen in other studies [11].

Whereas previously we considered the absolute value of the change in irradiance, we now take into account whether it is positive or negative. It can be seen in Fig. 10 that the satellite data agrees well with the station data, with the satellite data capturing a similar amount and magnitude of changes in irradiance.

5.3. Removal of diurnal cycle

The distribution of the changes in irradiance can be explained in part by the diurnal cycle. To reduce the diurnal cycles influence and analyze how well the satellite dataset predicts changes in irradiance that are not due to the diurnal cycle, it was removed from the data. This was achieved by dividing the satellite irradiance at each time by the corresponding clear sky radiation value [49,50]. The station data was normalized by the same values used for the satellite data to allow a direct comparison. The resulting output is a ratio of normalized irradiance, where values close to 1 indicate clear sky conditions and lower values indicate cloudy conditions. Changes in the normalized radiation occurring on a 15-min basis were then analyzed as described in Section 5.2. The hourly breakdown is shown in Fig. 11.

The changes have a more even distribution throughout the day for both datasets, with most small-scale changes (0–0.1) occurring around midday. Fig. 12 shows the sign of the change in normalized irradiance. Comparing this to Fig. 10, the normalized satellite data doesn't capture the frequency of changes in irradiance as accurately as when the diurnal cycle is present, however it still provides a good indication of the frequency of changes that occur. This is likely due to the difficulty in accurately modeling atmospheric attenuation.

5.4. Conversion of irradiance into power

The satellite dataset was converted into DC power at Kalaeloa for all available data to consider the dataset in terms of DC power. Fig. 13 shows yearly boxplots for Station 1 for irradiance and DC power. There is a large spread of data for each year, shown by the error bars, which reflects the seasonal variability seen in irradiance and resulting power. There is little variability seen in the mean irradiance or power between years, with the range of the mean being 70 W/m^2 and 0.23 kW respectively. This echoes the behavior seen in Fig. 7, where little variation is seen in the monthly diurnal cycles between each year.

Variation is more apparent when considering different months, shown in Fig. 14. The summer months show higher levels of irradiance and power produced, compared to the winter months due to increased cloud cover. This is reflected in the mean, with the range being larger at 240 W/m^2 and 0.56 kW. This behavior is seen in previous studies [6] as well as in Fig. 8, which both show summer months showing the higher levels of irradiance compared to winter.

To see how well the satellite data can capture variability between individual years, three years with different meteorological conditions were chosen. A La Nina and an El Nino year (2008 and 2015) were used to see if the satellite data is able to capture the

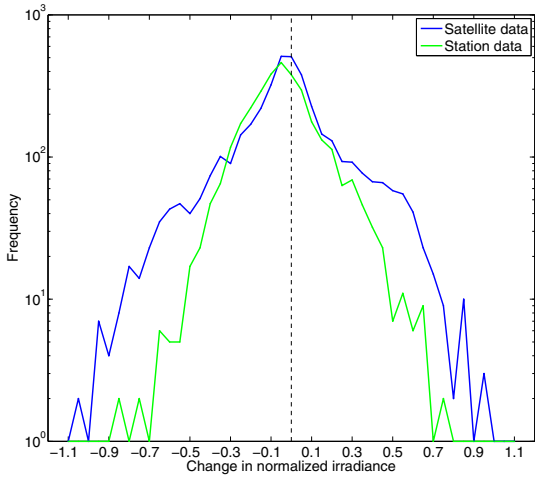

Fig. 12. Frequency of changes in normalized irradiance ordered by magnitude, showing type of change (positive or negative) for Station 1 in 2010 and 2011.

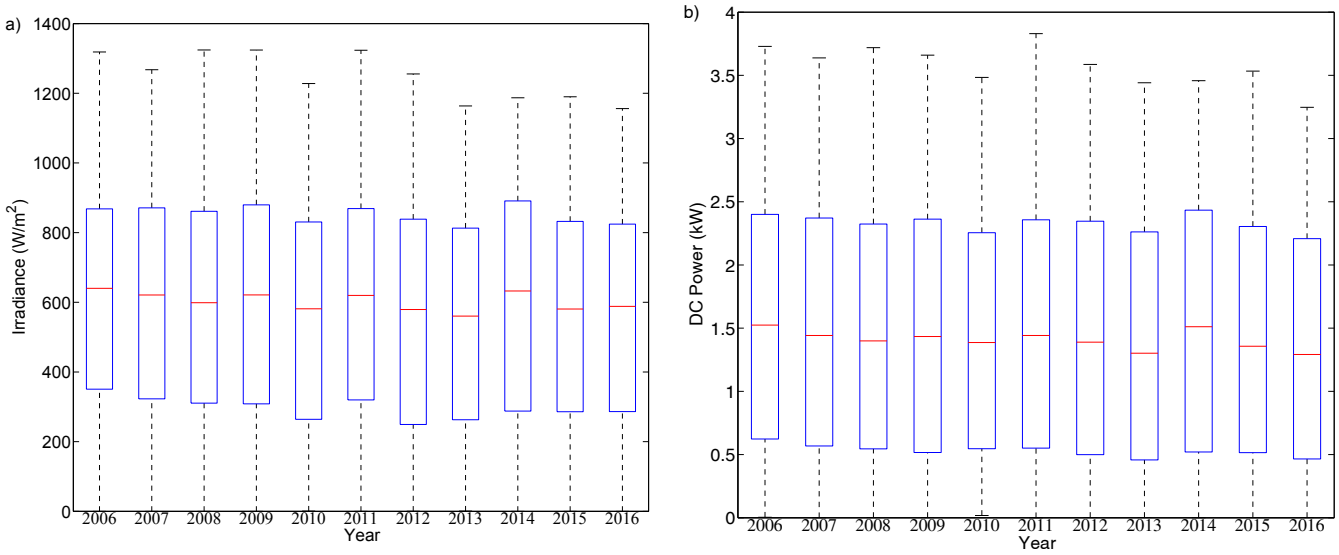

Fig. 13. Yearly boxplots for Station 1 for (a) satellite irradiance data and (b) power data for all years with available data.

difference between these two years. During a La Nina year, increased cloud cover and rainfall are expected, whilst during an El Nino year, drier conditions are typically seen. The year 2006 was also chosen due to the persistent occurrence of Kona lows during March and April, to see if it is contained in the satellite data.

Considering this in terms of power that would be generated from the satellite dataset, Fig. 15 shows the estimated weekly power generated for Station 1 for each of the years chosen. The Kona lows can be clearly seen, with lower amounts of power generated. Higher levels of irradiance are seen during 2015 compared to 2008, reflecting the drier conditions experienced during El Nino years.

6. Summary and conclusions

Surface irradiance is estimated from GOES-West imagery using the Heliosat method for Oahu, Hawai'i. We find that the satellite irradiance data performs well in comparison with previous studies, with RMSE values of 15–30%, compared with values of 20–25% [47], 17–25% [48] and 14–30% [32] found in literature. Additionally, CC values are consistently good ranging from 0.78 to 0.95. Correcting for viewing angle discrepancies, where possible, improves the performance of the satellite data, giving a mean RMSE value of 23.9% compared to 24.4% for periods without this correction. This shows the importance of taking into account and correcting for the effect of cloud shadows on surface irradiance.

Variability on sub hourly, diurnal, monthly and yearly timescales are captured within the irradiance dataset. The highest levels of irradiance occur around midday during the summer months whilst the lowest levels are seen during winter months. Varying amounts of cloud cover during the winter cause the variability during this time to be higher between the years, compared to the summer.

When considering sub-hourly variability, it was found that the majority of changes are of a small magnitude (0 W/m^2 to 200 W/m^2) and occur during the morning and afternoon, consistent with the diurnal cycle. Larger changes tend to occur around midday, indicating passing clouds. The removal of the diurnal cycle causes

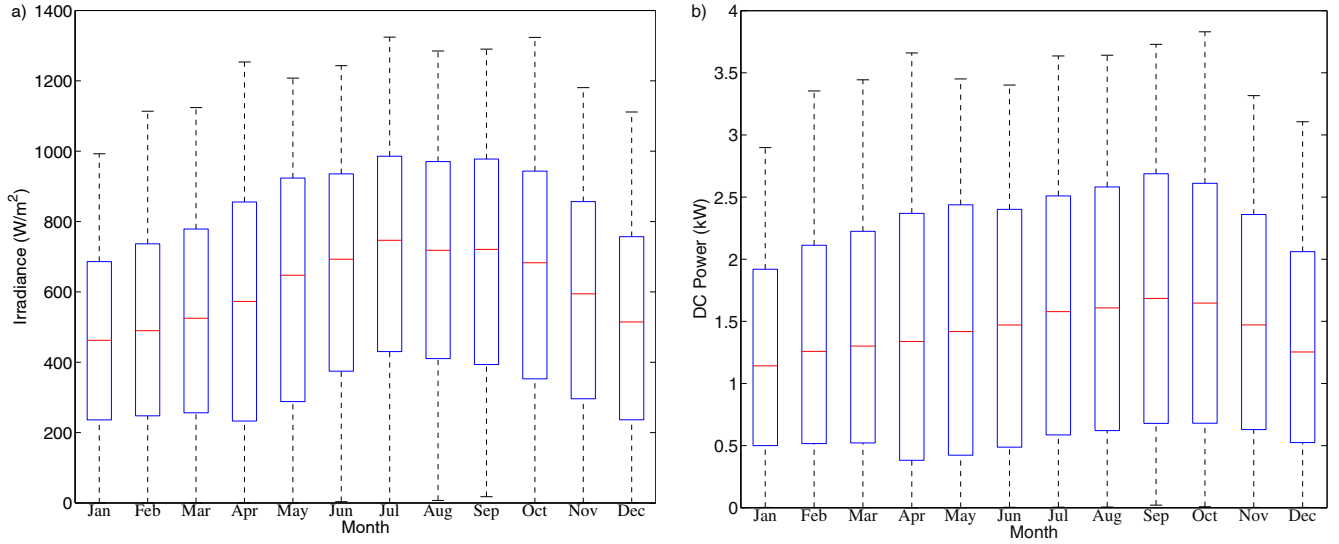

Fig. 14. Monthly boxplots for Station 1 for (a) satellite irradiance data and (b) power data for all years with available data.

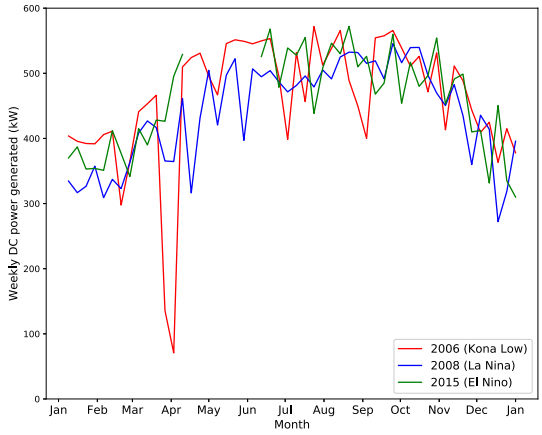

Fig. 15. Weekly DC power (kW) generated for Station 1 for 2006, 2008 and 2015. The sum of DC power was taken every 7 days and plotted through time for each year. Gaps indicate missing data.

changes to be distributed more evenly throughout the day, however the satellite data isn't as successful at capturing them compared to when the diurnal cycle is present.

In conclusion, variability on multiple time scales are contained within the satellite dataset, including events such as an El Nino year, a La Nina year and Kona lows, as well as a spatial distribution consistent with previous research. The dataset is successfully able to converted into power to show that it could be used as a historic dataset for modeling power generation.

Whilst the dataset has been shown to be usable for modeling power generation for a simplified system configuration, the next step would be to implement a more realistic configuration based on current Solar PV sites to assess how the dataset performs under these conditions. The irradiance dataset itself can also be improved and updated over time as more station observations become available, satellite measurement techniques are refined and methods are improved.

Acknowledgments

This work was supported by the US Dept. of Energy Cooperative Agreement DE-EE0003507, ONR Award N00014-18-1-2166 and the Hawaii State Barrel Tax - Environmental Response, Energy, and Food Security Tax. The authors would also like to thank John Cole, Richard Rocheleau and Kevin Davies from the Hawai'i Natural Energy Institute at the University of Hawai'i at Manoa, Derek Stenclik and Eduardo Ibanez from GE Energy Consulting, Randy Aliss from Northrop Grumman Corporation and Ryan Longman, Daniel Argueso and Lacey Holland from the University of Hawaii at Manoa for all their contributions towards this study.

References

[1] Hawai'i Natural Energy Institute, Oahu Wind Integration Study, 2011 (Technical Report).
[2] H.Z. Che, G.Y. Shi, X.Y. Zhang, R. Arimoto, J.Q. Zhao, L. Xu, B. Wang, Z.H. Chen, Analysis of 40 years of irradiance data from China, 1961–2000, Geophys. Res. Lett. 32 (2005) L06803.
[3] C.A. Gueymard, S.M. Wilcox, Assessment of spatial and temporal variability in the US solar resource from radiometer measurements and predictions from models using ground-based or satellite data, Sol. Energy 85 (2011) 51068–51084.
[4] B.W. Kariuki, T. Sato, Interannual and spatial variability of solar radiation energy potential in Kenya using Meteosat satellite, Renew. Energy 116 (A) (2018) 88–96.
[5] J. Polo, Solar global horizontal and direct normal irradiation maps in Spain derived from geostationary satellites, J. Atmos. Sol. Terr. Phys. 130–131 (2015) 81–88.
[6] R. Bryce, I.L. Carreño, A. Kumler, B. Hodge, B. Roberts, C.B. Martinez-Anido, Consequences of neglecting the interannual variability of the solar resource: a case study of photovoltaic power among the Hawaiian Islands, Sol. Energy 167 (2018) 61–75.
[7] E.G. Dutton, D.W. Nelson, R.S. Stone, D. Longnecker, G. Carbaugh, J.M. Harris, J. Wendell, Decadal variations in surface solar irradiance as observed in a globally remote network, J. Geophys. Res. (2006) 111.
[8] A. Ohmura, Observed decadal variations in surface irradiance and their causes, J. Geophys. Res. 114 (2009).
[9] M. Wild, H. Gilen, A. Roesch, A. Ohumura, C.N. Long, E.G. Dutton, F. Forgan, A. Kallis, V. Russak, A. Tsvetkov, From dimming to brightening; decadal changes in irradiance at Earth's surface, Science 308 (5723) (2005) 847–850.
[10] J.M. Vindel, J. Polo, Intermittency and variability of daily solar irradiation, Atmos. Res. 143 (2014) 313–327.
[11] D. Matthews, M. Dubarry, S. Busquet, K. Stein, R.E. Rocheleau, Characterizing solar irradiance observations in Hawai'i for application to solar power generation and forecasting, Renew. Energy (2014). Pre-print).
[12] R. Perez, S. Kivalov, J. Schlemmer, K. Hemker, T. Hoff, Parametrization of site-specific short-term irradiance variability, Sol. Energy 85 (2011) 1343–1353.
[13] Leopold, L.B., The interaction of trade wind and sea breeze, Hawai. J. Meteorol. 6, 5 312–320.
[14] T.W. Giambelluca, X. Shuai, M.L. Barnes, R.J. Alliss, R.J. Longman, T. Miura, Q. Chen, A.G. Frazier, R.G. Mudd, L. Cuo, A.D. Businger, Evapotranspiration of Hawai'i, Final report submitted to the U.S. Army Corps of Engineers—Honolulu District, and the Commission on Water Resource Management, State of Hawai'i, 2014.
[15] R. Smolarkiewicz, M. Rasmussen, T.L. Clark, On the dynamics of Hawaiian cloud bands: island forcing, J. Atmos. Sci. 45 (13) (1988) 1872–1905.
[16] R. Longman, T.W. Giambelluca, R.J. Alliss, M.L. Barnes, Temporal solar radiation change at high elevations in Hawai'i, J. Geophys. Res.: Atmosphere 119 (2014) 6022–6033.
[17] R. Longman, T.W. Giambelluca, A.G. Frazier, Modeling clear-sky solar radiation across a range of elevations in Hawai'i: comparing the use of input parameters at different temporal resolutions, J. Geophys. Res. 117 (2012).
[18] R. Longman, T.W. Giambelluca, M.A. Nullet, Use of clear-day solar radiation model to homogenize radiation measurements in Hawai'i, Sol. Energy 91 (2013) 102–110.
[19] R. Perez, R. Seals, A. Zelenka, Comparing satellite remote sensing and ground network measurements for the production of site/time specific irradiance data, Sol. Energy 60 (1997) 89–96.
[20] M. Sengupta, A. Habte, C. Gueymard, S. Wilbert, D. Renné, Best Practices Handbook for the Collection and Use of Solar Resource Data for Solar Energy Applications, second ed., NREL, 2017 technical report).
[21] J. Polo, S. Wilbert, J.A. Ruiz-Arias, R. Meyer, C. Gueymard, M. Súri, L. Martín, T. Mieslinger, P. Blanc, I. Grant, J. Boland, P. Ineichen, J. Remund, R. Escobar, A. Troccoli, M. Sengupta, K.P. Nielsen, D. Renne, N. Geuder, T. Cebecauer, Preliminary survey on site-adaptation techniques for satellite-derived and reanalysis solar radiation datasets, Sol. Energy 132 (2016) 25–37.
[22] M. Noia, C.F. Ratto, M. Festa, Solar irradiance estimation from geostationary satellite data: I. statistical models, Sol. Energy 51 (6) (1993) 449–456.
[23] M. Noia, C.F. Ratto, M. Festa, Solar irradiance estimation from geostationary satellite data: II. Physical models, Sol. Energy 51 (6) (1993) 457–465.
[24] C. Gautier, G. Diak, S. Masse, A simple physical model to estimate incident solar radiation at the surface from GOES satellite data, J. Appl. Meteorol. 19 (1980) 1005–1012.
[25] D. Cano, J.M. Monget, M. Albussion, H. Guillard, N. Regas, L. Wald, A method for the determination of global irradiance from meteorological satellite data, Sol. Energy 37 (1986) 31–39.
[26] R. Perez, P. Ineichen, K. Moore, M. Kmiecik, C. Chain, R. George, F. Vignola, A new operational model for satellite-derived irradiances: description and validation, Sol. Energy 73 (2002) 307–317.
[27] I. Pagola, M. Gaston, A. Bernardos, C. Fernandez-Peruchena, A combination of Heliosat-1 and Heliosat-2 methods for deriving irradiance from satellite images, Energy Procedia 57 (2014) 1037–1043.
[28] R.W. Mueller, K.F. Dagestad, P. Ineichen, M. Schroedter-Homscheidt, S. Cros, D. Dumortier, R. Kuhlemann, J.A. Olseth, G. Piernavieja, C. Reise, L. Wald, D. Heinemann, Rethinking satellite-based solar irradiance modeling: the SOLIS clear-sky module, Rem. Sens. Environ. 91 (2) (2004) 160–174.
[29] A. Hammer, C. Heinemann, R. Kuhlemann, E. Lorenz, R. Muller, H.G. Beyer, Solar energy assessment using remote sensing technologies, Rem. Sens. Environ. 86 (2003) 423–432.
[30] B.G. Akinoglu, S.E. Rusen, Combining the satellite imagery with bright sunshine hours: a review, J. Renew. Sustain. Energy 5 (2013) 041802.
[31] H.G. Beyer, C. Costanzo, Heinemann, Modifications of the Heliosat procedure for irradiance estimates from satellite data, Sol. Energy 56 (1996) 121–207.
[32] C. Rigollier, M. Lefe'vre, L. Wald, The method Heliosat-2 for deriving shortwave solar radiation from satellite images, Sol. Energy 77 (2004) 159–169.
[33] J. Page, Algorithms for the Satellight Programme, 1996 (Technical Report).
[34] D. Dumortier, Modeling Global and Diffuse Horizontal Irradiances under Cloudless Skies with Different Turbidities, vol. 2, Daylight II, 1995. Final Report.
[35] M. Fontoynont, D. Dumortier, D. Heinemann, A. Hammer, J. Olseth, A. Skartveit, P. Ineichen, C. Reise, J. Page, L. Roche, H.G. Beyer, L. Wald, Satellight—processing of METEOSAT Data for the Production of High Quality Daylight and Irradiance Available on a World Wide Web Internet Server, Mid-

term progress report JOR3-CT 95-0041, Project Satel-Light, for the Commission of the European Communities, 1997.
[36] System Advisory Model, https://sam.nrel.gov/, last accessed 08/22/17
[37] S.J. Nieman, J. Schmetz, W.P. Menzel, A comparison of several techniques to assign heights to cloud tracers, J. Appl. Meteorol. 32 (1993) 1559–1568.
[38] Remote Automatic Weather Stations, http://famit.nwcg.gov/applications/RAWS, last accessed 05/30/17.
[39] National Wildfire Coordinating Group, Interagency Wildland Fire and Weather Station Standards & Guidelines, 2014. PMS 426–3.
[40] R.J. Longman, T.W. Giambelluca, M.A. Nullet, A.G. Frazier, K. Kodama, S.D. Crausbay, P.D. Krushelnycky, S. Cordell, M.P. Clark, A.J. Newman, J.R. Arnold, Compilation of climate data from heterogeneous networks across the Hawaiian Islands, Scientific Data 5 (2018) 180012.
[41] https://midcdmz.nrel.gov/, last accessed 04/09/18
[42] M. Sengupta, A. Andreas, Oahu Solar Measurement Grid (1-Year Archive): 1-second Solar Irradiance, Oahu, Hawaii (Data), NREL, 2010. Report No. DA-5500–56506.
[43] S. Wilcox, A. Andreas, Solar Resource Meteorological Assessment Project (SOLRMAP): Rotating Shadowband Radiometer (RSR), Kalaeloa Oahu, Hawaii (Data), NREL, 2010. Report No. DA-5500–56497.
[44] Hawai'i Natural Energy Institute, Solar Resource and PV Systems Performance at Selected Test Sites, 2012 (Technical Report).
[45] MesoWest station weather observations, http://mesowest.utah.edu/, last accessed 06/16/17
[46] S.L. Barnes, Mesoscale Objective Map Analysis Using Weighted Time-series Observations, NOAA, National Severe Storms Laboratory, 1973.
[47] A. Zelenka, R. Perez, R. Seals, D. Renne, Effective accuracy of satellite-derived hourly irradiances, Theor. Appl. Climatol. 62 (1999) 199–207.
[48] Polo, J., Zarzalejo, L.F., Ramirez, L., Solar Radiation Derived from Satellite Images, 2008. Modeling Solar Radiation at the Earth's Surface, Chapter 18, Springer, Berlin, Heidelberg
[49] C.N. Long, T.P. Ackerman, Surface measurements of solar irradiance; a study of the spatial correlation between simultaneous measurements at separated sites, J. Appl. Meteorol. 34 (5) (1995) 1039–1046.
[50] C.W. Hansen, J.S. Stein, A. Ellis, Statistical Criteria for Characterizing Irradiance Time Series, 2010. Sandia Report, SAND2010–7314.